Nanocomposition of PEDOT:PSS with metal phthalocyanines as promising hole transport layers for organic photovoltaics

Xeniya Rozhkova [a], Aitbek Aimukhanov [a], Assylbek Zeinidenov [a], Vladimir Paygin [b], Damir Valiev [b], Juan Bisquert [c,d], Antonio Guerrero [c,*], Alexander Alexeev [a,e], Baurzhan Ilyassov [d,*]

[a] *Buketov University of Karaganda, Center of Nanotechnology and Functional Nanomaterials, University str., 28, 100028 Karaganda, Kazakhstan*
[b] *National Research Tomsk Polytechnic University, Lenin Avenue 30, 634050 Tomsk, Russia*
[c] *Institute of Advanced Materials (INAM), Universitat Jaume I, 12006 Castelló, Spain*
[d] *Astana IT University, 010000, Mangilik El, EXPO C1, Nur-Sultan, Kazakhstan*
[e] *Kazan Federal University, Kremlyovskaya street 18, 420008 Kazan, Russia*

ARTICLE INFO

ABSTRACT

PEDOT:PSS is one of the most widely used materials as a hole selective layer in organic photovoltaics due to its easy processing and high reproducibility. Unfortunately, the material is limited when testing new donor:acceptor systems due to its intrinsic frontier energy levels which typically leads to energy losses due to inadequate energy level alignment and presence of resistive losses. In this work, PEDOT:PSS:metal phthalocyanines nanocomposite thin films are formulated and used as hole transport layer for organic solar cells (OSCs). PEDOT:PSS is formulated with H_2Pc, CuPc, CoPc and ZnPc metal phthalocyanines (MPc) with nanobelt morphology which confers the compatibility with the active layer. Atomic force microscopy (AFM) and x-ray diffraction (XRD) were used to study the morphology and structure of nanocomposite films, respectively. OSCs based on PEDOT:PSS:MPc nanocomposite films were fabricated and the effect of hybrid hole transport layer with various phthalocyanines on photovoltaics properties was studied. Overall, nanocomposition of PEDOT:PSS with metal phthalocyanines improves the final power conversion efficiency of solar cells by 20% by a reduction of the resistive losses due to inadequate energy level alignment. The addition of metal phthalocyanines to PEDOT:PSS is a promising method for tailor-made hole transport materials for new donor:acceptor systems to improve their efficiencies.

1. Introduction

Nowadays, leading research groups around the world in the field of photovoltaics are making efforts to develop inexpensive, environmentally friendly and flexible organic solar cells (OSCs) [1–8]. OSC consists of several layers deposited on substrates coated with transparent conducting oxide (TCO) [9,10]. Usually, a photoactive bulk heterojunction layer, a mixture of a photoactive polymer and a fullerene derivative, is sandwiched between hole selective and electron selective layers. These selective contacts play a crucial role for a charge separation and transport to external electrodes. In traditional OSCs with a direct architecture, the widespread hole selective/transport layer (HTL) is a PEDOT: PSS polymer [11–13].

PEDOT:PSS has unique properties, which makes it so popular to use as HTL [14–17]. PEDOT:PSS thin film (~20–30 nm) has a relatively high optical transparency, hole conductivity and an appropriate thermal stability. PEDOT:PSS is also widely used in optoelectronic devices such as organic light emitting diodes (OLEDs) as HTL [18,19]. In addition, the properties of PEDOT:PSS are highly tunable being possible to modify the doping levels, conductivity and work function of the layers. For example, the processing conditions will determine the residual water content in the film and this will control the conductivity of the layers [20]. Thus, the charge transport properties of PEDOT:PSS thin films can be further improved by optimizing its structure and morphology [21–23]. Commonly, PEDOT:PSS thin films are deposited by a spin-coating technique from an aqueous solution. During the spin-coating deposition of PEDOT:PSS, PSS species tend to form agglomerates. PSS is dielectric in nature and its agglomeration in the film results in inhomogeneous out-of-plane conductivity and the rough surface [24–27].

To enhance the out-of-plane conductivity and reduce the surface roughness of PEDOT:PSS films, a number of methods were proposed. It is

---

a worth to mention the following methods such as chemical processing [28], post-processing [29,30], doping with organic nanostructures [31], developing composites [32]. One of the perspective ways to increase the power conversion efficiency of OPV is to embed various nanostructures in semiconducting polymers [28]. The modification of PEDOT:PSS structure improves the carrier transfer efficiency and as result PCE [33]. Doping polymeric charge transport layer with nanosized organic materials makes it possible to create a hybrid layer. In this hybrid layer the polymer material properties will be combined with the high optical and electrical properties of organic nanostructures. It should be noted that the fabrication of such composite materials is technologically simple and cost-effective process, which add the additional advantage for their use [34,35].

Metal phthalocyanines (MPc) are considered to be promising hole selective/transport materials for the application in organic and perovskite solar cells and light emitting diodes. They have relatively high hole mobility, catalytic activity, chemical and thermal stability [36]. Most of them easily form ordered nanostructures [37]. The incorporation of metal phthalocyanine nanostructures into the OPV photoactive layer results in the improvement in the polymer crystallinity, the charge carriers diffusion length, and enhances the charge carriers mobility [37]. The use of phthalocyanines alone as the hole-transport layer in organic solar cell instead of PEDOT:PSS leads to a decrease in the PCE of the solar cell. Whereas, the use of the PEDOT:PSS:MPc composite layer as the HTL layer improves the efficiency of the solar cell compared to individual components [38]. However, the effect of PEDOT:PSS doped with organic and inorganic nanostructures on morphological, optical, and electrical transport characteristics are not fully understood.

In this work, H$_2$Pc, CuPc, CoPc and ZnPc metal phthalocyanines nanobelts were synthesized by chemical vapor deposition (CVD). These phthalocyanines nanostructures were added to PEDOT:PSS solution and hybrid PEDOT:PSS:MPc nanocomposite thin films as hole transport layers for OSCs were deposited. The influence of MPc composition, hybrid HTL morphology and structure on charge transport and photovoltaics properties were studied in detail.

2. Materials and methods

2.1. Sample preparation procedure

Nanobelts of metal phthalocyanines (H$_2$Pc, CuPc, CoPc and ZnPc) were deposited on glass substrates by a chemical vapor deposition (CVD) [39]. The structural formulas of all used chemicals are presented in Fig. 1. Before the deposition, substrates were cleaned in acetone, 2-propanol and deionized water [40]. As-grown MPc nanobelts were mechanically scratched from substrates to 2-propanol in order to wash them. Then MPc 2-propanol suspension was centrifuged in order to precipitate MPc powders. The obtained MPc powders were dried and kept in a vial. The obtained MPc powders were directly added to aqueous PEDOT:PSS solution (Al4083, Ossila) and the solution was kept in ultrasonic bath in order to obtain a uniform and dispersed solution. The weight ratio of H$_2$Pc and MPc (CuPc, CoPc and ZnPc) was taken 5%, 10% and 15% which was chosen based on results of the several studies [37,38,41]. According to these studies if the MPc concentration exceeds 10w%, the film quality deteriorates and as a result PCE of device decreases. For more details on a MPc concentration optimization, readers can refer the study of X. Zhang and et al. [38].

The nanocomposite PEDOT:PSS:MPs HTL were spin-coated from the prepared solution (spin-coater SPIN150i Semiconductor Production System) at a rotation speed of 4000 rpm for 30 s. Then the substrates were annealed at a temperature of 120 °C for 10 min. The thickness of the nanocomposite HTLs film were in a 30–40 nm range.

The mixture of PTB7-TH:ITIC polymers in a ratio of 1:1.3 (Borun, 98%) was used as a donor and acceptor material to form bulk heterojunction active layer. PTB7-Th (~11 mg) was dissolved in 1 ml of chlorobenzene and the solution was stirred at 70 °C for 2 h. Then, ITIC (~14.4 mg) was added to the PTB7-Th solution. The solution was further stirred at 70 °C for 24 h. Before use, the solution was filtered through a 0.45 micrometer syringe filter. PTB7-Th:ITIC solution (25 μl) was spin-coated on FTO/glass substrates coated with PEDOT:PSS or PEDOT:PSS:MPs at a rotation speed of 2000 rpm for 30 s. At this rotation speed, PTB7-Th:ITIC photoactive layers have the thickness of 90–95 nm. Further, as-coated PTB7-Th:ITIC layers were annealed at 120 °C for 15 min to improve crystallinity. Finally, aluminum electrodes with thicknesses of 150 nm were deposited by thermal evaporation in vacuum of ~10^{-5} bar by using a CY-1700x-spc-2 sputtering setup (Zhengzhou CY Scientific Instruments Co., Ltd) at the evaporation rate of 2–3 nm/s. The evaporation was carried out using shadow masks to form four separate solar cells on a single substrate. The working area of each individual solar cell was 0.16 cm^2. Finally, the devices were encapsulated by using epoxy and cover glasses (Ossila) under the low intensity UV radiation ($\lambda = 315$ nm) for 5 – 10 min

2.2. Characterizations

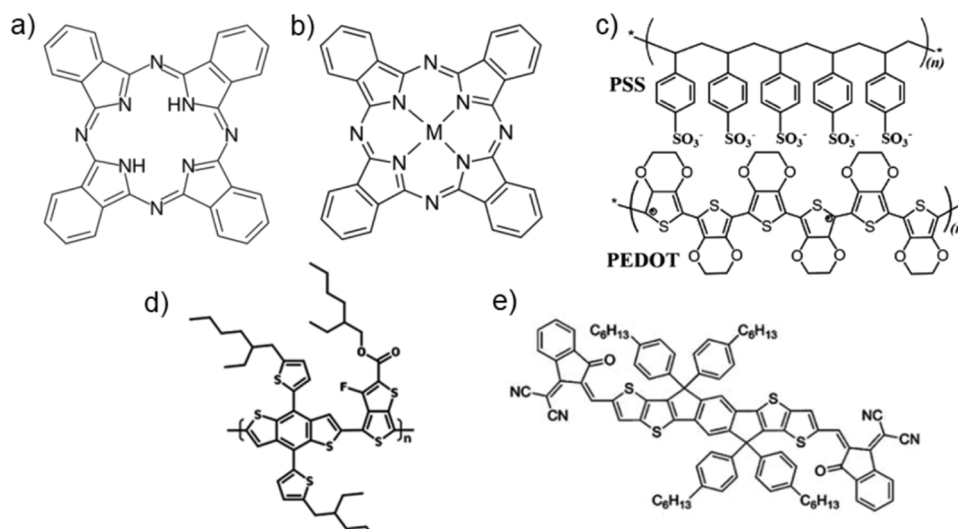The surface morphologies of thin films were studied by an atomic

Fig. 1. Structural formulas used chemicals: phthalocyanine (a) and its metal complexes (b) (where M is Cu, Co, Zn), PEDOT:PSS polymer (c), PTB7-Th donor (d) and ITIC non-fullerene acceptor (e).

force microscope (AFM) JSPM-5400 (JEOL, Japan) in semi-contact scanning mode. The surface morphology and roughness of nano-composite PEDOT:PSS thin films were analyzed by using the Winspm II Data Processing software package (JEOL Ltd). The grain size of thin films was determined using the ImageJ program.

The crystal structure of the samples was studied by X-Ray Diffraction (XRD) methods. XRD measurements were performed on an XRD-7000S Shimadzu diffractometer with CuKα radiation (Japan). The XRD scanning was in the range of 2θ from 5º to 30º with a step of 0.02º and a shutter speed at each step of 4 s. Diffraction patterns were decoded using the special software "Crystallographica Search-Match" and the "PDF-4″" international crystallographic database.

The absorption spectra of thin films were measured by an AvaSpec-ULS2048CL-EVO fiber spectrometer (Avantes), which records absorption spectra in the range of 200–2500 nm and has an optical resolution of 0.04 nm.

The I-V characteristics of the solar cells were measured by a PVIV-1A I-V station under a light illumination from a Sol3A solar simulator (AAA class, Newport) with an intensity of 100 mW/cm^2.

The impedance spectra of devices were measured by a P45X potentiostat (Elins) with a FRA module. The IS measurements were conducted in dark condition at varies bias voltage in the range of 0–1000 mV. Amplitude of perturbation signal was 30 mV and scanning range was from 100 kHz to 0.5 Hz. The fitting and analysis the impedance spectra was carried out by the EIS-analyzer software according to the method described in [42].

3. Results and discussion

3.1. Morphological characterizations

At the first step of this work, various metal phthalocyanine thin films with nanobelt morphology (H$_2$Pc, CuPc, CoPc and ZnPc) were synthesized by the CVD method [39]. The morphologies of synthesized metal phthalocyanine (MPc) thin films are shown in Fig. 2a-d. As can be seen from Fig. 2a-d, there is no any noticeable differences in the MPc morphologies. In average, the length and the diameter of MPc are 100 nm and 10 nm, respectively.

After CVD, in MPc were scratched from the substrate in 2-propanol (IPA) and the resulting solution was kept in an ultrasonic bath in order to obtain a dispersed solution. To confirm that in the dispersed IPA solution we still have MPc nanobelts, a drop of the solution was spin-coated on the FTO/glass substrate, dried and probed by AFM. AFM image of dispersed MPc nanobelts is shown in the Fig. 2e. It can be seen from the Fig. 2e that MPc persists the nanobelt morphology.

However, PEDOT:PSS is deposited from aqueous solution. Therefore, in order to check whether MPc structure is stable in water or not, after CVD deposition MPc nanobelts were released from substrate mechanically, washed in 2-propanol, dried and then transferred to water. As a next stage obtained dispersion was kept in an ultrasonic bath. Then, MPc aqueous solution was spin coated on the surface of FTO coated glass substrates and probed by AFM in tapping mode (Fig. 2.1a).

As can be seen from AFM images, MPc hardly sustain their initial morphology. Mostly we observe irregularly shaped crystal-like particles, which certainly means that crystalline structure is preserved. Initial nanobelt type morphology is still noticeable, however number of long crystals is far less of the initial amount (Fig. 2.1). In overall, we can conclude that MPc crystalline structure is relatively stable in aqueous solution, but initial long crystals are destroyed by sonication into small pieces.

The thickness of the obtained composite film was determined by using AFM equipped by stiff probe, which, at first, scanned surface in hard contact mode for producing step as it shown in Figure SI.1 (Supporting Information). After that the obtained step height was measured by AFM in tapping mode and its value was calculated from statistical analysis. The obtained value of the composite film thickness is 40 ± 3 nm, which is larger than average size of MPc particle, as it shown in Fig. 2.1. Some of the large MPc particles were also removed from dispersion by using filtration before deposition.

The precipitated MPc from 2-propanol was dried and added to a PEDOT:PSS aqueous solution and from this hybrid solution, PEDOT:PSS:MPc nanocomposite thin films were deposited by the spin-coating technique. The surface morphology of the pristine PEDOT:PSS and PEDOT:PSS:MPc nanocomposite thin films probed by AFM are illustrated in Fig. 2f-j. As can be observed from the AFM images, the nano-composition of PEDOT:PSS with MPc reduces the film roughness and the
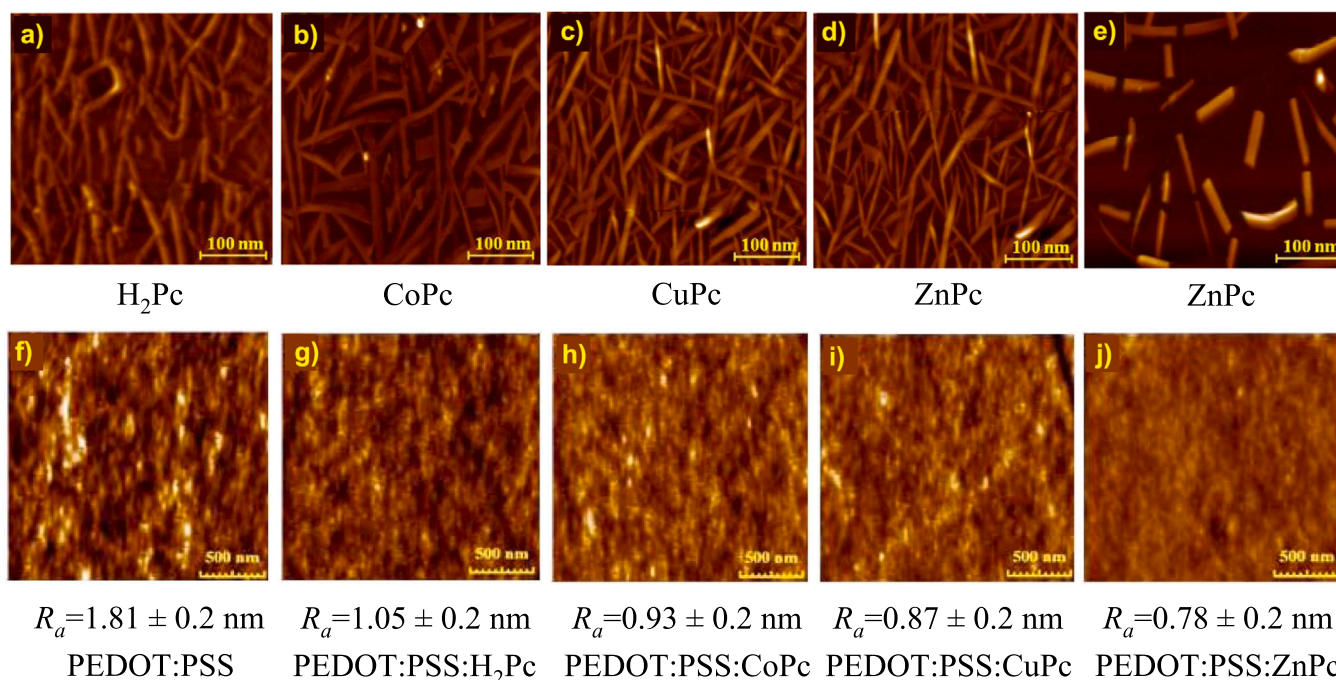

H$_2$Pc	CoPc	CuPc	ZnPc	ZnPc

R_a=1.81 ± 0.2 nm	R_a=1.05 ± 0.2 nm	R_a=0.93 ± 0.2 nm	R_a=0.87 ± 0.2 nm	R_a=0.78 ± 0.2 nm
PEDOT:PSS	PEDOT:PSS:H$_2$Pc	PEDOT:PSS:CoPc	PEDOT:PSS:CuPc	PEDOT:PSS:ZnPc

Fig. 2. AFM images of the studied films: (a-d) MPc films, (e) image of a dispersed ZnPc, (f) pristine PEDOT:PSS film and (g-j) PEDOT:PSS:MPc composites.
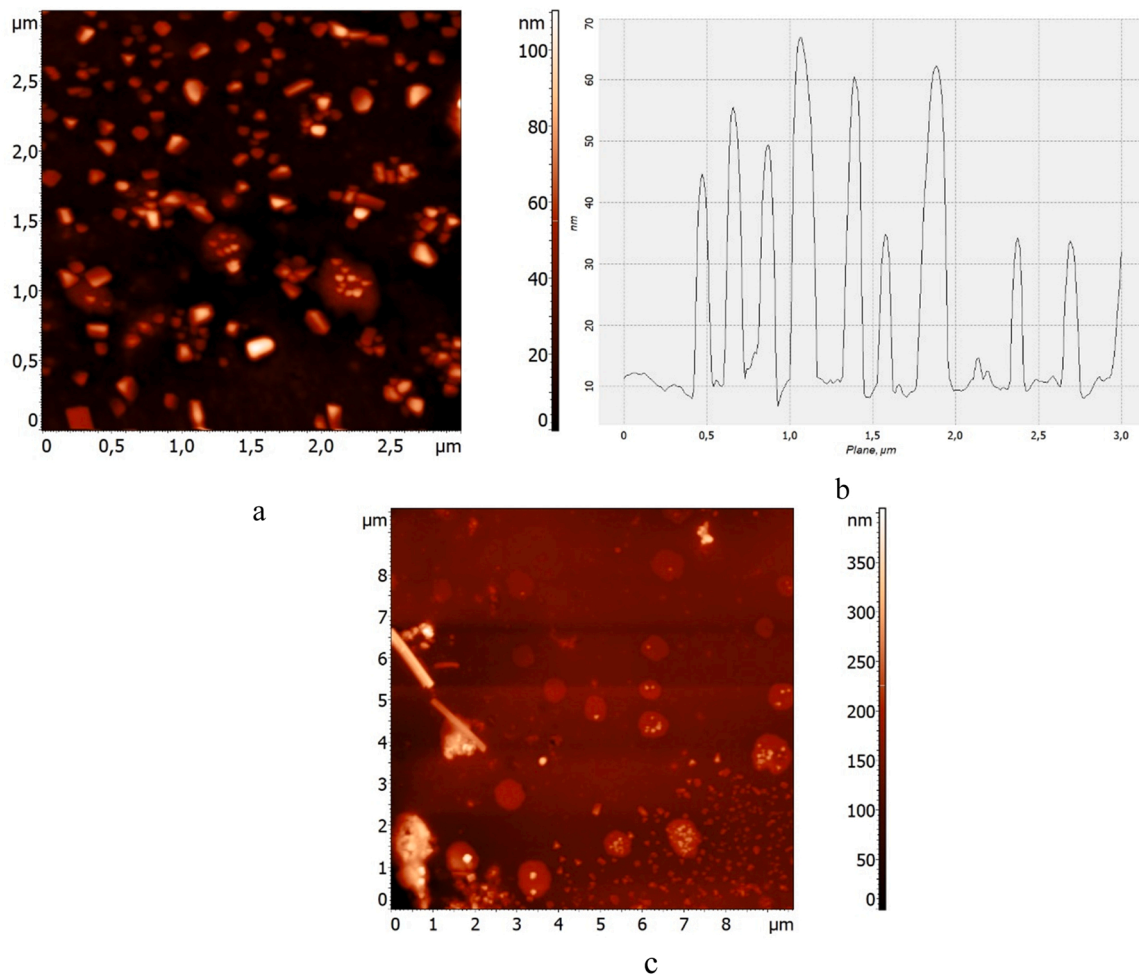
Fig. 2.1. AFM images of the surfaces of FTO coated by MPc aqueous solution.

pin-hole density. The pristine PEDOT:PSS film had the highest roughness, around 1.81 nm, and the highest density of pin-holes. We observe that the quality of the nanocomposite films improves in the following order: H_2Pc, CoPc, CuPc, and ZnPc. The PEDOT:PSS:ZnPc nanocomposite revealed the lowest roughness and pin-hole density, which is

beneficial for the formation of the high quality interface with a photoactive layer [43].

The observed improvements in the nanocomposite film morphology could be associated with the facilitation of solidification process. The dispersed MPc species can serve as nucleation centers and facilitate the
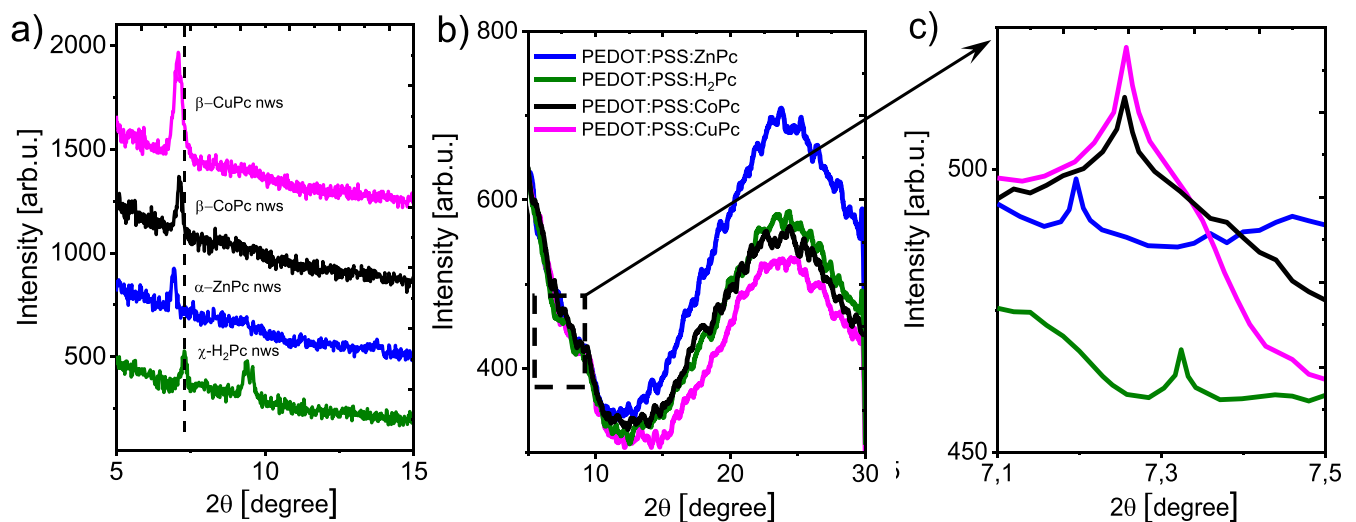

Fig. 3. XRD of H_2Pc and MPc phthalocyanine (a), PEDOT:PSS with H_2Pc and metal complexes CoPc, ZnPc, CuPc (b), enlarged image of a plot of phthalocyanine and metal complexes (c).

PEDOT:PSS solidification [44]. However, the process of nano-composition is beyond the scope our work.

3.2. XRD characterizations

Fig. 3a shows the X-Ray Diffraction (XRD) patterns of spectra of phthalocyanine nanobelts and its metal complexes. It is known that molecules of phthalocyanine and its metal complexes can form crystal structures in several modifications [45]. For example, the most common structures are thermally metastable α- and β-phases [45,46]. These phases differ from each other by different values of the tilt angle between the normal to the plane of the molecule. The figure shows that the diffraction pattern of metal-free phthalocyanine (H_2Pc) displaying two maxima at angles 7.28° and 9.41° (position along 2θ), which corresponds to the (200) and (100) diffraction planes. The position of the peaks corresponds to the reference diffraction pattern PDF-000–42–1889. Analysis of the diffraction peaks shows that H_2Pc molecules form nanobelts in the χ-phase [47,48].

Alternatively, CuPc and CoPc molecules in nanobelts take the form of the β-phase [49,50]. CuPc and CoPc nanobelts have one diffraction peak with a maximum at 7.09° and 7.10° angles, respectively, which corresponds to the diffraction plane (100). The ZnPc nanobelts have a diffraction maximum at a 2θ value of 6.94° in the (100) diffraction plane. Analysis of the diffraction pattern showed that ZnPc molecules in nanobelts are in the α phase (PDF 000–11–0714) [49]. Two diffuse halos are also observed in the diffraction patterns. Their presence can be explained by both amorphous and nanostructure phases in the samples. In addition, low-intensity crystalline peaks in the region of 7° and amorphous halos are observed in the diffraction patterns. It is worth mentioning that detailed study of phthalocyanine structure and its metal complexes is difficult procedure [51].

The Fig. 3b represents XRD pattern of PEDOT:PSS:MPc nano-composite thin films. The X-ray reflection spotted at 2θ ≈ 25.6° can be attributed to the distance between π-π stacking of the PEDOT chains [52]. Analysis of the XRD data of PEDOT:PSS with metal complexes of phthalocyanines shows that the intensity of the diffraction maximum of the studied samples depends on the type of doping phthalocyanine nanobelts (Fig. 3b). The maximum intensity is observed for films doped with pure phthalocyanine ZnPc. The lowest intensity value was recorded for copper phthalocyanine. It is known that for polymer structures based on PEDOT:PSS, the intensity indicates the degree of crystallinity of the film [37,41,49]. Thus, it can be assumed that the observed change in intensity is associated with the influence of MPc nanobelts on the interaction of π-π stacking of the PEDOT chains. For the pristine PEDOT:PSS film, we could not detect any XRD signal, which indicate about poor crystallinity of pure PEDOT:PSS film.

3.3. Optical properties

Fig. 4 shows the absorption spectra of the pristine PEDOT:PSS films and nanocomposite films. In the absorption spectra, we observe five absorption bands from the nanocomposite films, whereas from the pristine PEDOT:PSS film only two. All types of films show an absorption band with the maximum at $\lambda_1 = 224.1 \pm 3$ nm (Fig. 4, D_1). Additionally, a shoulder with a maximum at $\lambda_2 = 259.7 \pm 3$ nm is observed (Fig. 4, D_2). The nature of the latter band (the shoulder) is associated with the absorption of the PSS aromatic fragment [53]. In case of nanocomposite films, three additional bands appear in the spectra, corresponding to the absorption spectra of the B- and Q-bands of metal phthalocyanine [36, 37]. Absorption peak positions and optical density values estimated from the absorption spectra measurement are shown in Table 1. The PEDOT:PSS/ZnPc nanocomposite film revealed the highest intensity of the absorption bands related with MPc.
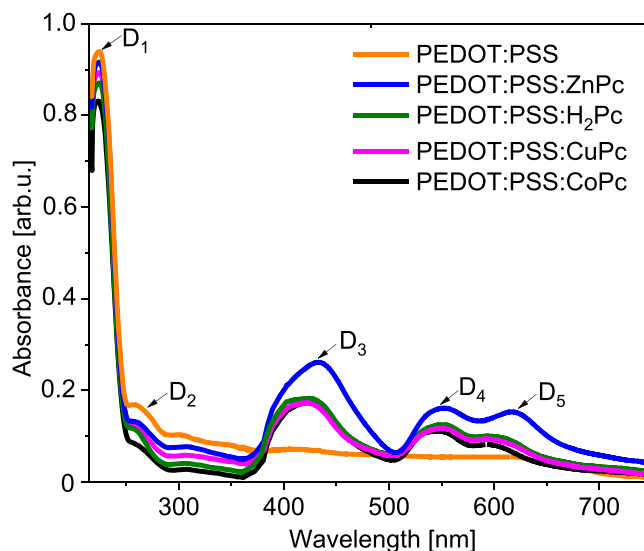

Fig. 4. Absorption spectra of PEDOT:PSS/MPc nanocomposite films.

3.4. Electro-physical properties

In order to understand the electronic properties of PEDOT:PSS nanocomposites with MPc complexes electronic devices were prepared and characterized by Impedance Spectroscopy (IS) in the dark using the architecture of FTO/PEDOT:PSS:PCs/Al. Note that the photovoltaic active layer is not included and only the contact layers are examined, since they contain the crucial electrical changes. Fig. 5 represents the measured (dotted lines) and the fitted (solid lines) impedance spectra of pristine and nanocomposite PEDOT:PSS films.

From the impedance spectrum it is observed that the data obtained at different frequencies form one arc and the equivalent circuit equivalent circuit shown in the inset may be used to fit the data [56,57]. Three electrical parameters can be evaluated using this circuit: 1-The series resistance of the device (R_s) that accounts from the resistance of the external contacts such as FTO, wires and other resistive layers that do not tend to store charge. 2-The resistance to the flow of current of the most resistive layer (R_1) and 3-The capacitance (C_1) connected to the charge stored in that layer. The latter two elements are connected in parallel and lifetime of carriers going across the resistive layer may be calculated as $\tau = R_1 C_1$. It is worth mentioning that FTO and Al are highly conductive materials typically used as current collectors, then, the most resistive layer must be the PEDOT:PSS.

A summary of the fitting results are shown in Table 2. From this data it is clear that the series resistance of the devices are the parameters that change the most when the different devices are compared. The reference device based on pristine PEDOT:PSS shows values of $R_s = 44$ Ω and values reduces when the different MPc are introduced into the blends with PEDOT:PSS:ZnPc revealing the lowest resistance of 14 Ω. Alternatively, the values for R_1 and C_1 are very similar for the complete set of devices and when a lifetime of the carriers is calculated the same $\tau = 0.02$ ms is obtained. Impedance spectra and fitted data of FTO/PEDOT:PSS/Al and FTO/PEDOT:PSS:ZnPc/Al devices measured at various bias voltages are shown in Figure SI.2 and Table SI.1 (Supporting Information). Overall, it can be concluded that the nano-composition of PEDOT:PSS with MPc complexes leads to the reduction in the series resistance of the devices. However, the resistance R_1 associated to PEDOT:PSS will act as a series resistance in the solar cells and have a deleterious effect in the fill factor.

The trend observed in series resistance in this simplified device configuration should be held once the active layer is used into the photovoltaic configuration. There are different proposals for the improved out of plane conductivity of nanocomposite films, especially

Table 1
The absorption spectra characteristics of PEDOT:PSS nanocomposite films.

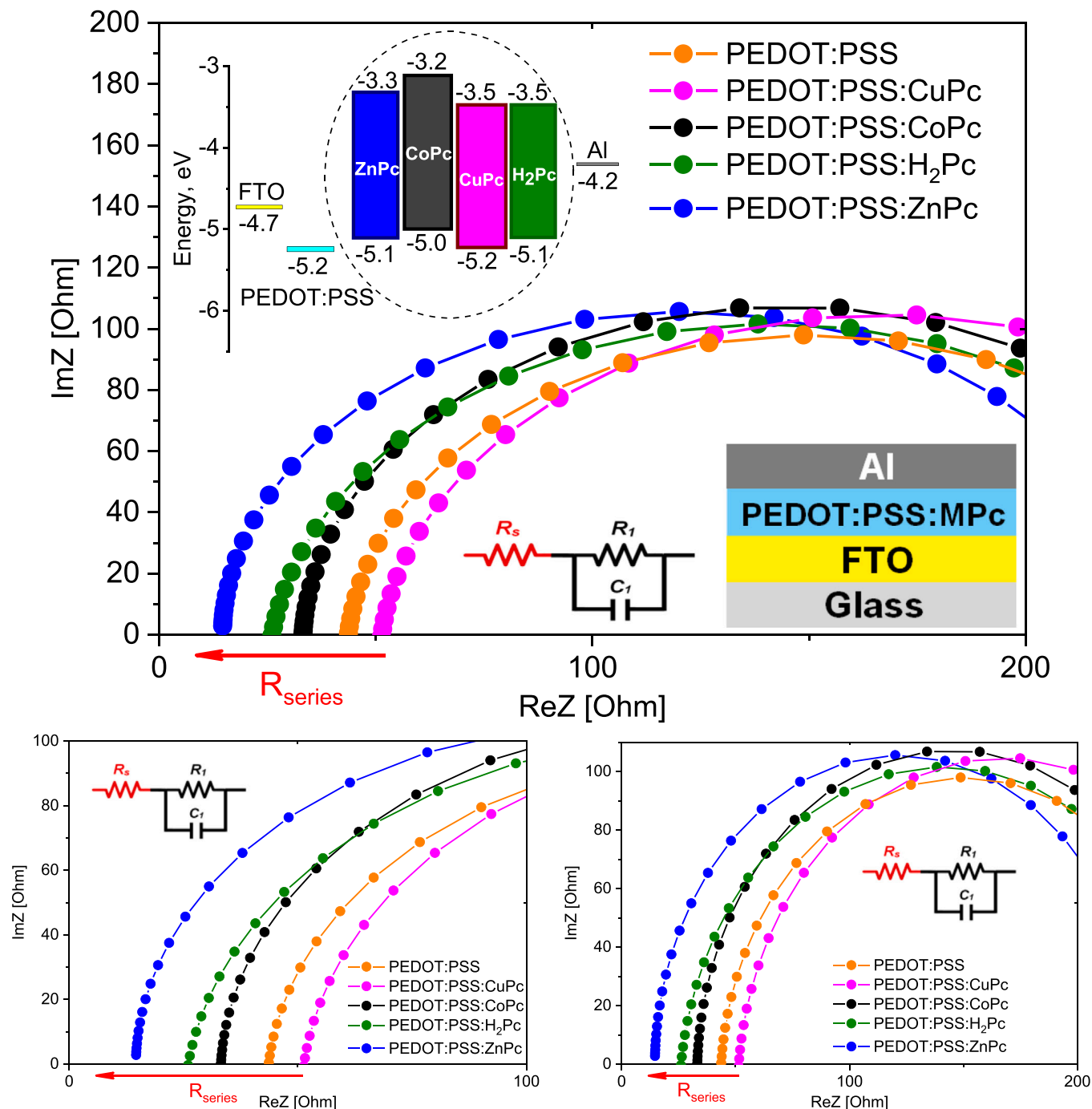| Sample	Absorption peaks		D_1, a.u.	D_2, a.u.	Absorption peaks			D_3, a.u.	D_4, a.u.	D_5, a.u.
	λ_1, nm	λ_2, nm			λ_3, nm	λ_4, nm	λ_5, nm			
PEDOT:PSS	224.1	259.7	0.94	0.17	-	-	-	-	-	-
PEDOT:PSS:ZnPc	223.9	259.7	0.92	0.14	434.1	551.5	617.8	0.26	0.17	0.16
PEDOT:PSS:H$_2$Pc	223.8	259.7	0.87	0.11	420.1	551.5	605.4	0.19	0.12	0.10
PEDOT:PSS:CuPc	223.9	259.7	0.89	0.12	419.9	548.7	602.4	0.18	0.11	0.09
PEDOT:PSS:CoPc	223.8	259.7	0.80	0.08	419.9	548.5	607.8	0.18	0.11	0.08

Fig. 5. Impedance spectra of FTO/PEDOT:PSS:MPc/Al devices, equivalent electrical circuit, energy levels diagram [36,37,54,55].

Table 2
Summary of impedance parameters obtained from nanocomposite films.

Sample	R_s (Ω)	R_1 (Ω)	C_1 (10^{-5}F)	τ (ms)
PEDOT:PSS	44	213	7.98	0.017
PEDOT:PSS:CuPc	53	246	7.31	0.018
PEDOT:PSS:CoPc	33	232	7.76	0.018
PEDOT:PSS:H$_2$Pc	26	225	8.45	0.019
PEDOT:PSS:ZnPc	14	221	9,05	0.020

*IS was measured at the bias voltage of 0.8 V

PEDOT:PSS:ZnPc can be explained by the presence of additional charge transport channels. For example, MPc species could serve as additional charge transport channels through which holes can directly diffuse to the electrode. Whereas, the slightly hindered charge transfer resistance at the interface we attribute with not optimized energy alignment [58].

3.5. Photovoltaic properties

OSCs based on the PEDOT:PSS:MPc nanocomposites were fabricated. Fig. 6 shows an OSC architecture consisting of several layers: a FTO covered glass substrate, the PEDOT:PSS/MPc nanocomposite layer; photoactive layer based on PTB7-Th:ITIC bulk heterojunction and aluminum cathode. The energy diagram of FTO/PEDOT:PSS:MPc/PTB7-Th:ITIC/Al is shown in Fig. 6, which was adopted from the works [59–61]. The current-voltage characteristics of the fabricated OSCs are illustrated in Fig. 6. From the current-voltage characteristics, photovoltaic performances of the devices were calculated and are listed in Table 3.

Nanocomposition of PEDOT:PSS with phthalocyanine affects the photovoltaic performance of OPV. The photovoltaic parameters of fabricated OPV are shown in Table 3. Results are in line with other reports based on the regular configuration terminated with an Aluminum contact without a buffer layer i.e. PDIN on the cathode side [62].

From Table 3, it can be seen that nanocomposition of PEDOT:PSS with MPc, except with CuPc, boosted PCE due to the improved short-circuit current density (J_{SC}) and open-circuit voltage (V_{OC}). The enhancement in J_{SC} is consistent with the reduction of series resistance of the devices due to the nanocomposition of PEDOT:PSS with MPc

determined from IS data. However, there is no similar trend in fill factor (*FF*) dynamic. Device *FF* is affected not only by HTL, it depends on each transport layers and interface properties. In sum, we can conclude that nanocomposition of PEDOT:PSS with MPc positively affect the device performance. The most profound effect is detected for OPV based on PEDOT:PSS:ZnPc nanocomposite. The champion device reached the PCE as high as 5.06%. The advantage of ZnPc can be understood from AFM, XRD and IS data. According to AFM images, PEDOT:PSS:ZnPc nanocomposite showed the lowest roughness, which is beneficial for photoactive layer crystallization and facilitates the formation of the optimal HTL/photoactive layer interface. The XRD response from PEDOT:PSS:ZnPc films was more intense, which indicates about the better crystallinity of PEDOT:PSS. IS study revealed that the series resistance of the device with PEDOT:PSS:ZnPc is lower in comparison with pristine PEDOT:PSS and other PEDOT:PSS:MPc nanocomposite films.

The series resistance of a solar cell can be evaluated from IV curve [63–67]. We calculated R_s of our OPV devices from IV data (Table 3) in order to compare with R_s of PEDOT:PSS cells evaluated from IS measurement. As can be seen from Table 3 the trend in R_s of OPV cells has similar trend as in the case with R_s of PEDOT:PSS cell (Table 2), which confirms that introduction of MPc in PEDOT:PSS improves its conductivity.

Further, we investigated the photostability characteristics of the OPV device based on PEDOT:PSS:ZnPc HTL and for the comparison the device based on pristine PEDOT:PSS HTL. For it, both types of devices were placed in a glovebox filled and uninterruptedly illuminated during 120 under AM1.5 light. Their performance was measured every hour [68].

The Fig. 7 shows the degradation evolution of PCE and FF. As can be seen from the Fig. 7 during the first 24 h PCE and FF falls faster losing about 30% of their initial values. Further, the degradation evolution is slower for both types of the devices. It is noticeable a slight improved photostability of the PEDOT:PSS:ZnPc based device, however it is not profound.

Finally, to optimize the device performance ETL was introduced. LiF layer (2–3 nm thick) was thermally evaporated before cathode deposition. The IV curve and photovoltaic characteristics of the OPV devices are shown Fig. 8 and in Table 4. As expected devices with LiF ETL demonstrated improved photovoltaic characteristics. The J_{SC}, V_{OC}, FF and PCE of OPV device based on pristine PEDOT:PSS increased by 2.4%,
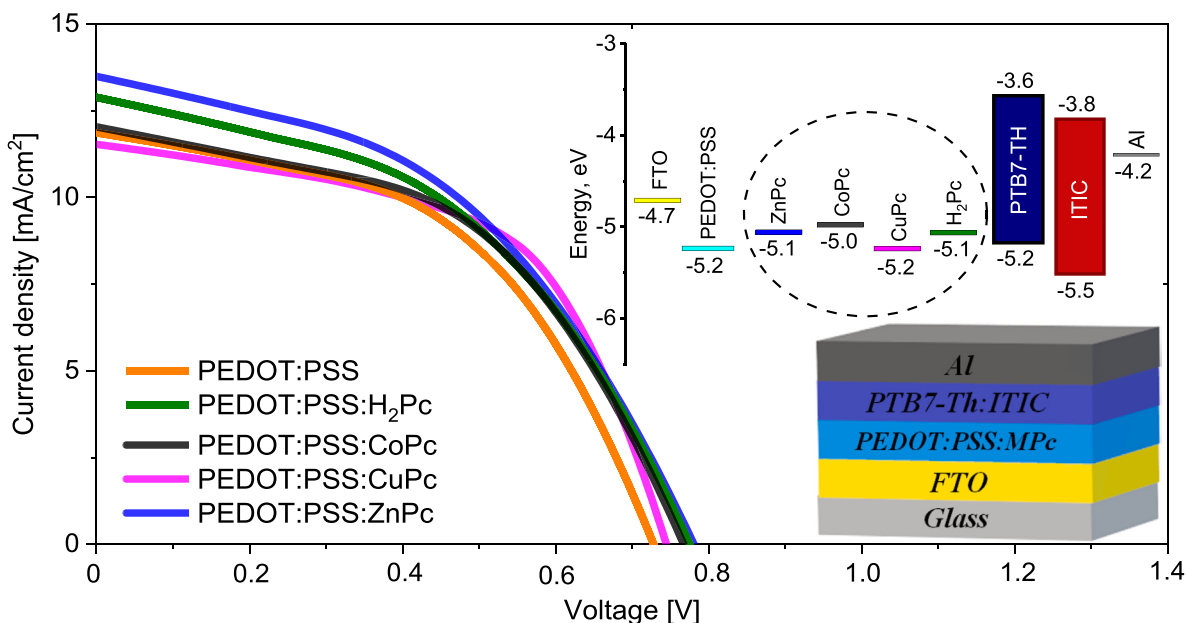

Fig. 6. Current-voltage characteristics, energy levels diagram and schematic structure of the solar cells with FTO/PEDOT:PSS:MPc/PTB7-Th:ITIC/Al composite hole-transport layer.

Table 3
Photovoltaic performance of FTO/PEDOT:PSS/MPc/PTB7:ITIC/Al organic solar cells.

| Sample	J_{sc} (mA/cm^2)	J_{max} (mA/cm^2)	V_{oc} (V)	V_{max} (V)	Fill Factor	Efficiency %	R_s Ω
PEDOT:PSS	11.93 ± 0.05	8.32 ± 0.05	0.73 ± 0.01	0.51 ± 0.01	0.46 ± 0.01	4.24 ± 0.05	45,2 ± 0.05
PEDOT:PSS:CuPc	11.35 ± 0.05	8.32 ± 0.05	0.75 ± 0.01	0.52 ± 0.01	0.51 ± 0.01	4.33 ± 0.05	54,3 ± 0.05
PEDOT:PSS:CoPc	11.95 ± 0.05	8.34 ± 0.05	0.77 ± 0.01	0.55 ± 0.01	0.49 ± 0.01	4.51 ± 0.05	33,1 ± 0.05
PEDOT:PSS:H$_2$Pc	12.87 ± 0.05	8.33 ± 0.05	0.76 ± 0.01	0.56 ± 0.01	0.48 ± 0.01	4.66 ± 0.05	25,7 ± 0.05
PEDOT:PSS:ZnPc	13.54 ± 0.05	8.73 ± 0.05	0.78 ± 0.01	0.58 ± 0.01	0.48 ± 0.01	5.06 ± 0.05	14,2 ± 0.05
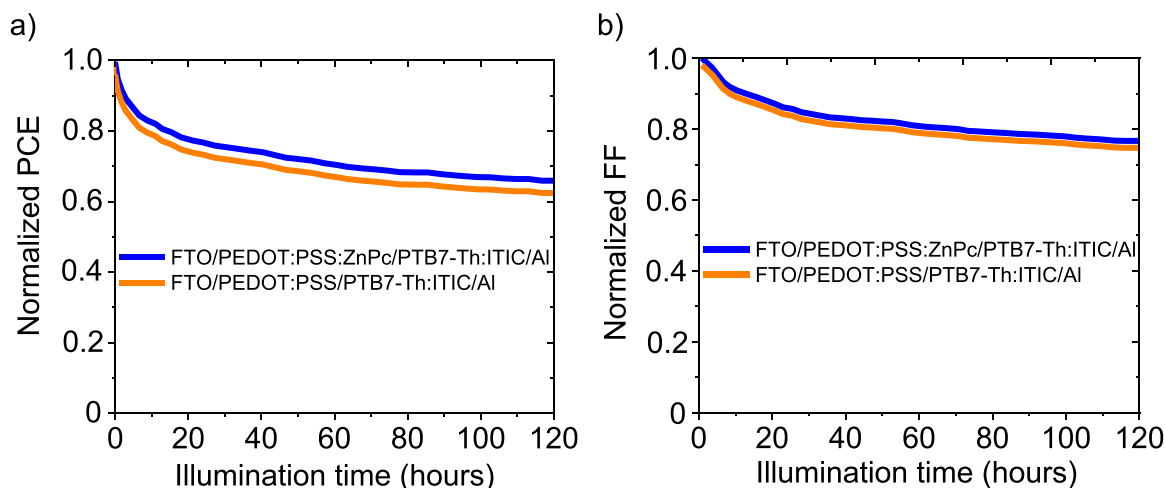
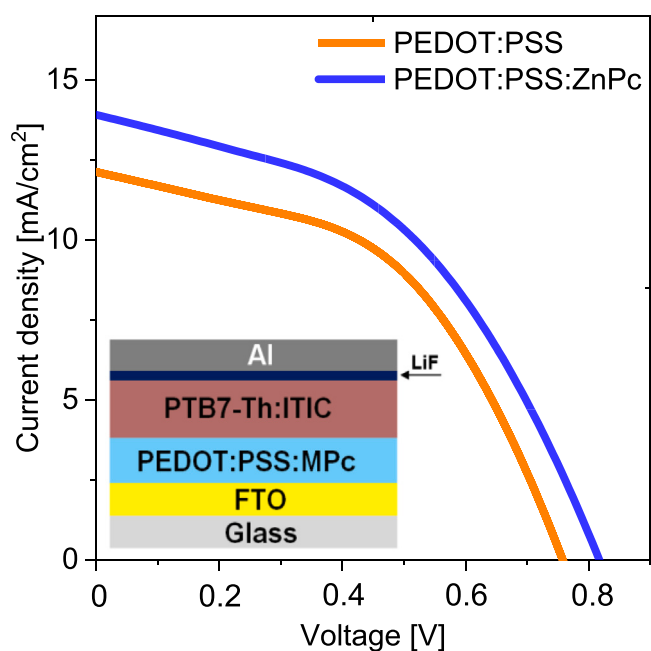**Fig. 7.** Photostability of investigated devices.

Fig. 8. I-V curves of solar cells FTO/PEDOT:PSS:MPc/PTB7-Th:ITIC/ LiF/Al.

Table 4
Photovoltaic performance of FTO/PEDOT:PSS:MPc/PTB7:ITIC/LiF/Al organic solar cells.

Sample	J_{sc} (mA/cm^2)	J_{max} (mA/cm^2)	V_{oc} (V)	V_{max} (V)	Fill Factor	Efficiency, %
PEDOT: PSS	12.22 ± 0.05	8.49 ± 0.05	0.75 ± 0.01	0.54 ± 0.01	0.50 ± 0.01	4.58 ± 0.05
PEDOT: PSS: ZnPc	13.87 ± 0.05	9.18 ± 0.05	0.81 ± 0.01	0.62 ± 0.01	0.51 ± 0.01	5.72 ± 0.05

4. Conclusion

In this work, the effect of nanocomposition of PEDOT:PSS with metal phthalocyanines on charge transport and photovoltaic properties of organic solar cells was studied. Four types of phthalocyanines (H$_2$Pc, CuPc, CoPc and ZnPc) with nanobelt morphology were synthesized by the chemical vapor deposition method. As-grown MPc nanobelts were dispersed in 2-proponol and added to PEDOT:PSS aqueous solution. From the prepared solution, PEDOT:PSS:MPc nanocomposite films were deposited by spin-coating methods. AFM and XRD study showed that adding MPc in PEDOT:PSS reduces the HTL roughness and pin-hole density, and improves film crystallinity. Among PEDOT:PSS:MPc nanocomposites, ZnPc based film revealed the lowest roughness and pin-hole density, and the highest crystallinity. PEDOT:PSS:MPc nano-composite films were used to as hole transport layers for organic solar cells. Impedance spectroscopy technique was used in order to study electric properties of PEDOT:PSS:MPc nanocomposite films. IS spectra of FTO/PEDOT:PSS:MPc/Al devices showed that nanocomposition of PEDOT:PSS with metal phthalocyanines result leads in the reduction of the series resistance and ZnPc based device showed the lowest series resistance. Organic solar cells with PEDOT:PSS:MPc nanocomposite films serving as HTL were fabricated. IV characterization indicated that

2.7%, 8.7% and 8%, respectively, due to the introduction of LiF ETL. In the case of OPV device based on PEDOT:PSS:ZnPc, the improvements is larger, and J_{SC}, V_{OC}, *FF* and PCE were boosted by 2.4%, 3.8%, 6.3% и 13%, respectively.

OPV devices with PEDOT:PSS:MPc nanocomposites have boosted photovoltaic performance except of CuPc based device. As it was expected OPV device with ZnPc revealed the highest performance mostly due to the improved short-circuit current density. The improved short-circuit current density of OPV based on PEDOT:PSS:MPc nanocomposites in comparison with pristine PEDOT:PSS can be attributed with improved HTL crystallinity, lower HTL roughness and the lower series resistance of the devices.

Declaration of Competing Interest

Data Availability

Data will be made available on request.

Acknowledgments

Appendix A. Supporting information

Supplementary data associated with this article can be found in the online version at doi:10.1016/j.synthmet.2023.117347.

References

[1] K.S. Schanze, P.V. Kamat, P. Yang, J. Bisquert, Progress in perovskite photocatalysis, ACS Energy Lett. 5 (2020) 2602–2604, https://doi.org/10.1021/acsenergylett.0c01480.
[2] Q. Cao, Y. Li, H. Zhang, J. Yang, J. Han, T. Xu, S. Wang, Z. Wang, B. Gao, J. Zhao, X. Li, X. Ma, S.M. Zakeeruddin, W.E.I. Sha, X. Li, M. Grätzel, Efficient and stable inverted perovskite solar cells with very high fill factors via incorporation of star-shaped polymer, Sci. Adv. 7 (2021), https://doi.org/10.1126/sciadv.abg0633.
[3] C. Lee, S. Lee, G.-U. Kim, W. Lee, B.J. Kim, Recent advances, design guidelines, and prospects of all-polymer solar cells, Chem. Rev. 119 (2019) 8028–8086, https://doi.org/10.1021/acs.chemrev.9b00044.
[4] L.X. Chen, Organic solar cells: recent progress and challenges, ACS Energy Lett. 4 (2019) 2537–2539, https://doi.org/10.1021/acsenergylett.9b02071.
[5] H. Chen, R. Zhang, X. Chen, G. Zeng, L. Kobera, S. Abbrent, B. Zhang, W. Chen, G. Xu, J. Oh, S.-H. Kang, S. Chen, C. Yang, J. Brus, J. Hou, F. Gao, Y. Li, Y. Li, A guest-assisted molecular-organization approach for >17% efficiency organic solar cells using environmentally friendly solvents, Nat. Energy 6 (2021) 1045–1053, https://doi.org/10.1038/s41560-021-00923-5.
[6] G. Zeng, W. Chen, X. Chen, Y. Hu, Y. Chen, B. Zhang, H. Chen, W. Sun, Y. Shen, Y. Li, F. Yan, Y. Li, Realizing 17.5% efficiency flexible organic solar cells via atomic-level chemical welding of silver nanowire electrodes, J. Am. Chem. Soc. 144 (2022) 8658–8668, https://doi.org/10.1021/jacs.2c01503.
[7] W. Sun, H. Chen, B. Zhang, Q. Cheng, H. Yang, Z. Chen, G. Zeng, J. Ding, W. Chen, Y. Li, Host-guest active layer enabling annealing-free, nonhalogenated green solvent processing for high-performance organic solar cells †, Chin. J. Chem. 40 (2022) 2963–2972, https://doi.org/10.1002/cjoc.202200437.
[8] B. Zhang, F. Yang, S. Chen, H. Chen, G. Zeng, Y. Shen, Y. Li, Y. Li, Fluid mechanics inspired sequential blade-coating for high-performance large-area organic solar modules, Adv. Funct. Mater. 32 (2022), 2202011, https://doi.org/10.1002/adfm.202202011.
[9] A. Stadler, Transparent conducting oxides—an up-to-date overview, Materials 5 (2012) 661–683, https://doi.org/10.3390/ma5040661.
[10] R. Xu, L. Min, Z. Qi, X. Zhang, J. Jian, Y. Ji, F. Qian, J. Fan, C. Kan, H. Wang, W. Tian, L. Li, W. Li, H. Yang, Perovskite transparent conducting oxide for the design of a transparent, flexible, and self-powered perovskite photodetector, ACS

Appl. Mater. Interfaces 12 (2020) 16462–16468, https://doi.org/10.1021/acsami.0c01298.
[11] C.J. Ko, Y.K. Lin, F.C. Chen, C.W. Chu, Modified buffer layers for polymer photovoltaic devices, Appl. Phys. Lett. 90 (2007) 1–4, https://doi.org/10.1063/1.2437703.
[12] J. Bouclé, S. Chyla, M.S.P. Shaffer, J.R. Durrant, D.D.C. Bradley, J. Nelson, Hybrid solar cells from a blend of poly(3-hexylthiophene) and ligand-capped TiO2 nanorods, Adv. Funct. Mater. 18 (2008) 622–633, https://doi.org/10.1002/adfm.200700280.
[13] K.X. Steirer, M.O. Reese, B.L. Rupert, N. Kopidakis, D.C. Olson, R.T. Collins, D.S. Ginley, Ultrasonic spray deposition for production of organic solar cells, Sol. Energy Mater. Sol. Cells 93 (2009) 447–453, https://doi.org/10.1016/j.solmat.2008.10.026.
[14] J. Li, J. Liu, C. Gao, J. Zhang, H. Sun, Influence of MWCNTs doping on the structure and properties of PEDOT:PSS films, Int. J. Photo 2009 (2009) 1–5, https://doi.org/10.1155/2009/650509.
[15] Y. fei Zhou, Y. bo Yuan, L. fang Cao, J. Zhang, H. qi Pang, J. rong Lian, X. Zhou, Improved stability of OLEDs with mild oxygen plasma treated PEDOT:PSS, J. Lumin. 122–123 (2007) 602–604, https://doi.org/10.1016/j.jlumin.2006.01.236.
[16] T.C. Tsai, W.Y. Hung, L.C. Chi, K.T. Wong, C.C. Hsieh, P.T. Chou, A new ambipolar blue emitter for NTSC standard blue organic light-emitting device, Org. Electron. 10 (2009) 158–162, https://doi.org/10.1016/j.orgel.2008.10.017.
[17] A.R.Paolo Vacca, Mario Petrosino, Riccardo Miscioscia, Giuseppe Nenna, Carla Minarini, Dario della Sala, Poly(3,4-ethylenedioxythiophene):poly(4-styrenesulfonate) ratio: Structural, physical and hole injection properties in organic light emitting diodes, Thin Solid Films 516 (2008) 4232–4237, https://doi.org/10.1016/j.tsf.2007.12.143.
[18] M.A. Leaf, M. Muthukumar, Electrostatic effect on the solution structure and dynamics of PEDOT:PSS, Macromolecules 49 (2016) 4286–4294, https://doi.org/10.1021/acs.macromol.6b00740.
[19] S. Mahato, L.G. Gerling, C. Voz, R. Alcubilla, J. Puigdollers, PEDOT:PSS as an alternative hole selective contact for ITO-free hybrid crystalline silicon solar cell, IEEE J. Photovolt. 6 (2016) 934–939, https://doi.org/10.1109/JPHOTOV.2016.2557072.
[20] J. Huang, P.F. Miller, J.S. Wilson, A.J. de Mello, J.C. de Mello, D.D.C. Bradley, Investigation of the effects of doping and post-deposition treatments on the conductivity, morphology, and work function of poly(3,4-ethylenedioxythiophene)/Poly(styrene sulfonate) films, Adv. Funct. Mater. 15 (2005) 290–296, https://doi.org/10.1002/adfm.200400073.
[21] J. Ouyang, C.W. Chu, F.C. Chen, Q. Xu, Y. Yang, High-conductivity poly(3,4-ethylenedioxythiophene):poly(styrene sulfonate) film and its application in polymer optoelectronic devices, Adv. Funct. Mater. 15 (2005) 203–208, https://doi.org/10.1002/adfm.200400016.
[22] F.J. Lim, K. Ananthanarayanan, J. Luther, G.W. Ho, Influence of a novel fluorosurfactant modified PEDOT:PSS hole transport layer on the performance of inverted organic solar cells, J. Mater. Chem. 22 (2012) 25057–25064, https://doi.org/10.1039/c2jm35646e.
[23] V.D. Mihailetchi, J.K.J. van Duren, P.W.M. Blom, J.C. Hummelen, R.A.J. Janssen, J.M. Kroon, M.T. Rispens, W.J.H. Verhees, M.M. Wienk, Electron transport in a methanofullerene, Adv. Funct. Mater. 13 (2003) 43–46, https://doi.org/10.1002/adfm.200390004.
[24] D.Y. Lee, S.I. Na, S.S. Kim, Graphene oxide/PEDOT:PSS composite hole transport layer for efficient and stable planar heterojunction perovskite solar cells, Nanoscale 8 (2016) 1513–1522, https://doi.org/10.1039/c5nr05271h.
[25] A. Giuri, S. Masi, S. Colella, A. Kovtun, S. Dell'Elce, E. Treossi, A. Liscio, C. Esposito Corcione, A. Rizzo, A. Listorti, Cooperative effect of GO and glucose on PEDOT:PSS for high VOC and hysteresis-free solution-processed perovskite solar cells, Adv. Funct. Mater. 26 (2016) 6985–6994, https://doi.org/10.1002/adfm.201603023.
[26] D. Huang, T. Goh, J. Kong, Y. Zheng, S. Zhao, Z. Xu, A.D. Taylor, Perovskite solar cells with a DMSO-treated PEDOT:PSS hole transport layer exhibit higher photovoltaic performance and enhanced durability, Nanoscale 9 (2017) 4236–4243, https://doi.org/10.1039/c6nr08375g.
[27] L. Hu, K. Sun, M. Wang, W. Chen, B. Yang, J. Fu, Z. Xiong, X. Li, X. Tang, Z. Zang, S. Zhang, L. Sun, M. Li, Inverted planar perovskite solar cells with a high fill factor and negligible hysteresis by the dual effect of NaCl-Doped PEDOT:PSS, ACS Appl. Mater. Interfaces 9 (2017) 43902–43909, https://doi.org/10.1021/acsami.7b14592.
[28] Y. Xia, S. Dai, Review on applications of PEDOTs and PEDOT:PSS in perovskite solar cells, J. Mater. Sci. Mater. Electron. 32 (2021) 12746–12757, https://doi.org/10.1007/s10854-020-03473-w.
[29] G. Namkoong, E.M. Younes, T.M. Abdel-Fattah, E.M. El-Maghraby, A.H. Elsayed, A.H.Abo Elazm, Aging process of PEDOT:PSS dispersion and robust recovery of aged PEDOT:PSS as a hole transport layer for organic solar cells, Org. Electron. 25 (2015) 237–244, https://doi.org/10.1016/j.orgel.2015.06.049.
[30] Y.H. Kim, C. Sachse, M.L. MacHala, C. May, L. Müller-Meskamp, K. Leo, Highly conductive PEDOT:PSS electrode with optimized solvent and thermal post-treatment for ITO-free organic solar cells, Adv. Funct. Mater. 21 (2011) 1076–1081, https://doi.org/10.1002/adfm.201002290.
[31] R. Bhujel, S. Rai, U. Deka, G. Sarkar, J. Biswas, B.P. Swain, Bandgap engineering of PEDOT:PSS/rGO a hole transport layer for SiNWs hybrid solar cells, Bull. Mater. Sci. 44 (2021), https://doi.org/10.1007/s12034-021-02376-8.
[32] Y. Yang, H. Deng, Q. Fu, Recent progress on PEDOT:PSS based polymer blends and composites for flexible electronics and thermoelectric devices, Mater. Chem. Front. 4 (2020) 3130–3152, https://doi.org/10.1039/d0qm00308e.

[33] A.K. Aimukhanov, X.S. Rozhkova, B.R. Ilyassov, A.K. Zeinidenov, N. Nuraje, The influence of structural and charge transport properties of <scp>PEDOT</scp>: <scp>PSS</scp> layers on the photovoltaic properties of polymer solar cells, Polym. Adv. Technol. 32 (2021) 497–504, https://doi.org/10.1002/pat.5102.

[34] H. Wang, D. Li, Y. Yuan, F. Chi, L. Liu, L. Wang, Z. Lu, Z. Lin, X. Zhang, Solution-processed WS 2 and its doping in PEDOT:PSS for tailoring hole injection in near ultraviolet organic light-emitting diodes, Appl. Opt. 60 (2021) 2610, https://doi.org/10.1364/AO.419279.

[35] L.N.Yuying Wang, Na Li, Mengqi Cui, Yuting Li, Xia Tian, Xijie Xu, Qikun Rong, Dong Yuan, Guofu Zhou, High-performance hole transport layer based on WS2 doped PEDOT:PSS for organic solar cells, Org. Electron. 99 (2021), 106305, https://doi.org/10.1016/j.orgel.2021.106305.

[36] A. Aimukhanov, A. Zeinidenov, A. Zavgorodniy, Influence of the size effect on the generation and transport of charge carriers of phthalocyanines, Opt. Mater. (Amst.). 116 (2021), 111099, https://doi.org/10.1016/j.optmat.2021.111099.

[37] A.K. Zeinidenov, A.K. Aimukhanov, D.S. Kambar, B.R. Ilyassov, A.V. Zavgorodniy, Effects of phthalocyanine nanostructure on photovoltaic performance of its polymer composite thin films, Mater. Chem. Phys. 267 (2021), 124680, https://doi.org/10.1016/j.matchemphys.2021.124680.

[38] X.-F. Zhang, X. Zhou, L. Zhang, B. Xu, Facile phthalocyanine doping into PEDOT leads to highly efficient and stable inverted metal halide perovskite solar cells, J. Mater. Chem. A 6 (2018) 12515–12522, https://doi.org/10.1039/C8TA03541E.

[39] K.S. Sree Harsha, Principles of Vapor Deposition of Thin Films, Elsevier S, Elsevier, 2006. ⟨https://doi.org/10.1016/B978-0-08-044699-8.X5000-1⟩.

[40] K. Kim, K. Ihm, B. Kim, Surface property of indium tin oxide (ITO) after various methods of cleaning, in: Acta Phys. Pol. A, 2015: pp. 1176–1179. ⟨https://doi.org/10.12693/APhysPolA.127.1176⟩.

[41] Y. Zhang, Z. Wei, Enhancing the performance of polymer solar cells using CuPc nanocrystals as additives, Nanotechnology 26 (2015), 204001, https://doi.org/10.1088/0957-4484/26/20/204001.

[42] J. Bisquert, I. Mora-Sero, F. Fabregat-Santiago, Diffusion-recombination impedance model for solar cells with disorder and nonlinear recombination, ChemElectroChem 1 (2014) 1–9, https://doi.org/10.1002/celc.201300091.

[43] Y.S. Kim, E.J. Lee, J.T. Lee, D.K. Hwang, W.K. Choi, J.Y. Kim, High-performance flexible transparent electrode films based on silver nanowire-PEDOT:PSS hybrid-gels, RSC Adv. 6 (2016) 64428–64433, https://doi.org/10.1039/c6ra06590b.

[44] Y. Liu, D. Sun, S. Askari, J. Patel, M. Macias-Montero, S. Mitra, R. Zhang, W.-F. Lin, D. Mariotti, P. Maguire, Enhanced Dispersion of TiO2 Nanoparticles in a TiO2/PEDOT:PSS Hybrid Nanocomposite via Plasma-Liquid Interactions, Sci. Rep. 5 (2015) 15765, https://doi.org/10.1038/srep15765.

[45] S. Yim, S. Heutz, T.S. Jones, Model for the α→β1 phase transition in phthalocyanine thin films, J. Appl. Phys. 91 (2002) 3632–3636, https://doi.org/10.1063/1.1446218.

[46] P. Keeratithiwakorn, P. Songkeaw, K. Onlaor, B. Tunhoo, Structural properties of copper phthalocyanine films grown by electrophoretic deposition process, Mater. Today Proc. 4 (2017) 6194–6199, https://doi.org/10.1016/j.matpr.2017.06.115.

[47] R.B. Hammond, K.J. Roberts, R. Docherty, M. Edmondson, R. Gairns, X-Form metal-free phthalocyanine: crystal structure determination using a combination of high-resolution X-ray powder diffraction and molecular modelling techniques, J. Chem. Soc. Perkin Trans. 2 (1996) 1527, https://doi.org/10.1039/p29960001527.

[48] X. Zhang, J. Tong, L. Ruan, X. Yao, L. Zhou, F. Tian, G. Qin, Interface hybridization and spin filter effect in metal-free phthalocyanine spin valves, Phys. Chem. Chem. Phys. 22 (2020) 11663–11670, https://doi.org/10.1039/D0CP00651C.

[49] H. Wang, S. Mauthoor, S. Din, J.A. Gardener, R. Chang, M. Warner, G. Aeppli, D. W. McComb, M.P. Ryan, W. Wu, A.J. Fisher, M. Stoneham, S. Heutz, Ultralong copper phthalocyanine nanowires with new crystal structure and broad optical absorption, ACS Nano 4 (2010) 3921–3926, https://doi.org/10.1021/nn100782w.

[50] P. Ballirano, R. Caminiti, C. Ercolani, A. Maras, M.A. Orrù, X-ray Powder Diffraction Structure Reinvestigation of the α and β Forms of Cobalt Phthalocyanine and Kinetics of the α → β Phase Transition, J. Am. Chem. Soc. 120 (1998) 12798–12807, https://doi.org/10.1021/ja973815p.

[51] C.W. Miller, A. Sharoni, G. Liu, C.N. Colesniuc, B. Fruhberger, I.K. Schuller, Quantitative structural analysis of organic thin films: an x-ray diffraction study, Phys. Rev. B. 72 (2005), 104113, https://doi.org/10.1103/PhysRevB.72.104113.

[52] X. Wang, A.K.K. Kyaw, C. Yin, F. Wang, Q. Zhu, T. Tang, P.I. Yee, J. Xu, Enhancement of thermoelectric performance of PEDOT:PSS films by post-treatment with a superacid, RSC Adv. 8 (2018) 18334–18340, https://doi.org/10.1039/C8RA02058B.

[53] Y. Xia, K. Sun, J. Ouyang, Highly conductive poly(3,4-ethylenedioxythiophene): poly(styrene sulfonate) films treated with an amphiphilic fluoro compound as the transparent electrode of polymer solar cells, Energy Environ. Sci. 5 (2012) 5325–5332, https://doi.org/10.1039/C1EE02475B.

[54] Z. Liu, X. Zhang, Y. Zhang, J. Jiang, Theoretical investigation of the molecular, electronic structures and vibrational spectra of a series of first transition metal phthalocyanines, Spectrochim. Acta Part A Mol. Biomol. Spectrosc. 67 (2007) 1232–1246, https://doi.org/10.1016/j.saa.2006.10.013.

[55] M.E. Azim-Araghi, J. Baedi, L. Moazzami Goodarzi, Electrical and optical properties of an organic semiconductor metal-free phthalocyanine (C 32H 18 N 8), Eur. Phys. J. Appl. Phys. 58 (2012) 30201, https://doi.org/10.1051/epjap/2012120062.

[56] G. Garcia-Belmonte, A. Munar, E.M. Barea, J. Bisquert, I. Ugarte, R. Pacios, Charge carrier mobility and lifetime of organic bulk heterojunctions analyzed by impedance spectroscopy, Org. Electron. 9 (2008) 847–851, https://doi.org/10.1016/j.orgel.2008.06.007.

[57] A. Guerrero, S. Loser, G. Garcia-Belmonte, C.J. Bruns, J. Smith, H. Miyauchi, S. I. Stupp, J. Bisquert, T.J. Marks, Solution-processed small molecule:fullerene bulk-heterojunction solar cells: impedance spectroscopy deduced bulk and interfacial limits to fill-factors, Phys. Chem. Chem. Phys. 15 (2013) 16456, https://doi.org/10.1039/c3cp52363b.

[58] L. Huang, D. Zhang, S. Bu, R. Peng, Q. Wei, Z. Ge, Synergistic interface energy band alignment optimization and defect passivation toward efficient and simple-structured perovskite solar cell, Adv. Sci. 7 (2020), 1902656, https://doi.org/10.1002/advs.201902656.

[59] S. Baba, A. Suzuki, T. Oku, Electronic structures and magnetic/optical properties of metal phthalocyanine complexes, in: A.I.P. Conf. Proc., 2016: p. 020012. ⟨https://doi.org/10.1063/1.4941211⟩.

[60] H.S. Nalwa, The effect of central metal atom on the electrical properties of phthalocyanine macromolecule, J. Electron. Mater. 17 (1988) 291–295, https://doi.org/10.1007/BF02652168.

[61] A.V. Vannikov, A.D. Grishina, Y.G. Gorbunova, V.I. Zolotarevskii, T.V. Krivenko, A. S. Laryushkin, L.A. Lapkina, V.V. Savel'ev, A.Y. Tsivadze, Influence of heavy central atom on photoelectric, nonlinear optical, and photorefractive properties of metal phthalocyanines, High. Energy Chem. 49 (2015) 36–43, https://doi.org/10.1134/S0018143915010142.

[62] Y. Lin, J. Wang, Z.-G. Zhang, H. Bai, Y. Li, D. Zhu, X. Zhan, An electron acceptor challenging fullerenes for efficient polymer solar cells, Adv. Mater. 27 (2015) 1170–1174, https://doi.org/10.1002/adma.201404317.

[63] M. Diantoro, T. Suprayogi, A. Hidayat, A. Taufiq, A. Fuad, R. Suryana, Shockley's equation fit analyses for solar cell parameters from I-V curves, Int. J. Photo 2018 (2018) 1–7, https://doi.org/10.1155/2018/9214820.

[64] M.S. Benghanem, S.N. Alamri, Modeling of photovoltaic module and experimental determination of serial resistance, J. Taibah Univ. Sci. 2 (2009) 94–105, https://doi.org/10.1016/S1658-3655(12)60012-0.

[65] A. Zekry, A.Y. Al-Mazroo, A distributed SPICE-model of a solar cell, IEEE Trans. Electron Devices 43 (1996) 691–700, https://doi.org/10.1109/16.491244.

[66] J.D. Servaites, S. Yeganeh, T.J. Marks, M.A. Ratner, Efficiency enhancement in organic photovoltaic cells: consequences of optimizing series resistance, Adv. Funct. Mater. 20 (2010) 97–104, https://doi.org/10.1002/adfm.200901107.

[67] D.S.H. Chan, J.C.H. Phang, Analytical methods for the extraction of solar-cell single- and double-diode model parameters from I-V characteristics, IEEE Trans. Electron Devices 34 (1987) 286–293, https://doi.org/10.1109/T-ED.1987.22920.

[68] A.J. Clarke, J. Luke, R. Meitzner, J. Wu, Y. Wang, H.K.H. Lee, E.M. Speller, H. Bristow, H. Cha, M.J. Newman, K. Hooper, A. Evans, F. Gao, H. Hoppe, I. McCulloch, U.S. Schubert, T.M. Watson, J.R. Durrant, W.C. Tsoi, J.-S. Kim, Z. Li, Non-fullerene acceptor photostability and its impact on organic solar cell lifetime, Cell Rep. Phys. Sci. 2 (2021), 100498, https://doi.org/10.1016/j.xcrp.2021.100498.